A novel hybrid supercapacitor based on spherical activated carbon and spherical MnO_2 in a non-aqueous electrolyte

Hong-Qiang Wang,[a] Ze-Sheng Li,*[a] You-Guo Huang,[a] Qing-Yu Li*[a] and Xin-Yu Wang[b]

Received 7th January 2010, Accepted 15th February 2010
First published as an Advance Article on the web 26th March 2010
DOI: 10.1039/c000339e

A novel non-aqueous hybrid supercapacitor was fabricated from two spherical materials – an activated mesocarbon microbead (AMCMB) and MnO_2 nanowire-sphere, as the negative and positive electrodes, respectively. The preliminary results for this energy-storage device, which operates over a wide voltage range (0.0–3.0 V) using 1 M Et_4NBF_4 in acetonitrile (AN) as electrolytes, are presented. On the basis of a single electrode, the AMCMB|MnO_2 supercapacitor displays a high specific capacitance of 228 F g^{-1} at a scan rate of 10 mV s^{-1}, corresponding to specific energy of 128 W h kg^{-1} based on based on the total mass of active materials, while maintaining desirable cycling stability and rate capability. The combination of the spherical AMCMB and MnO_2 in a non-aqueous electrolyte is proved to be suitable for high-performance hybrid supercapacitor applications.

1. Introduction

Supercapacitors or electrochemical capacitors are promising devices for energy storage in a wide range of applications, such as hybrid electric vehicles, electronic devices and memory backup systems, where high power density and long cycle-life are desirable.[1] Generally, supercapacitors (electrochemical double-layer capacitors, EDLCs) are mainly based on two symmetric activated carbon electrodes (AC|AC) in aqueous electrolytes. However, it is difficult for such supercapacitors to achieve higher specific energy with higher operating voltage required for new applications, due to the limit of low double-layer capacitance of activated carbon and the low electrochemical window (~1.23 V) of water.[2] Typical commercial EDLCs have specific energies of 5–10 W h kg^{-1}, while Li-ion batteries have achieved energy densities as high as 150 W h kg^{-1}.[3]

Recently, a new non-aqueous hybrid supercapacitor that typically consists of an activated carbon (AC) negative electrode and a metal oxide (MO) positive electrode, such as AC|NiO and AC|TiO_2 systems,[4] was found to be an effective approach to increase the specific energy of supercapacitors. It was believed that, different from the AC|AC aqueous system, the high pseudo-capacitance of the metal oxide electrode associated with the potentially large operational voltage window (2–4 V) of the organic electrolyte could result in a significant increase in the overall specific energy of hybrid supercapacitors, based on the formula $E = \frac{1}{2}CV^2$. For instance, Wang and co-workers fabricated a TiO_2/CNT hybrid supercapacitor with a reported specific energy of 12.5 W h kg^{-1}, double the value of the CNT/CNT symmetric supercapacitor.[4c] In addition, a hybrid energy storage device using TiO_2 (B) as the negative electrode and activated carbon as the positive electrode was also assembled which exhibited an extremely high specific energy of 80 W h kg^{-1} according to the total mass of active materials.[5]

Although increasing the specific energy is an important consideration, retaining high power density is also crucial for supercapacitor applications. Generally, most of these MO|AC hybrid supercapacitors are based on a common non-aqueous medium, namely a lithium salt ($LiPF_6$) dissolved in organic solvents (ethylene carbonate, dimethyl carbonate, propylene carbonate, *etc.*). The decomposition voltage of this organic electrolyte can reach 4 V, but the ionic conductivity is usually low, which precludes reaching high powers easily.[6] In recent years, another non-aqueous electrolyte, Et_4NBF_4 dissolved in acetonitrile (AN), began to be used for high power performance EDLCs due to its high ionic conductivity and wide electrochemical stability window.[7] However, to our knowledge, MO|AC hybrid supercapacitors using Et_4NBF_4 as electrolyte have not been reported yet, although these seem to be very attractive devices to achieve both high specific energy and specific power, which is one novelty of the current work.

The selection and assembly of electrode materials in favorable morphologies have been considered as central issues in the development of energy storage applications,[8] with spherical materials showing great advantages over other morphologies (*e.g.* irregular materials).[9] The most outstanding advantage is the high packing density, which is very important for increasing the specific energy. These materials also have excellent dispersivity and fluidity, leading to high performances in electrode manufacturing. As a result, much effort has been devoted to the development of spherical electrode materials in energy storage applications.[10] The present work presents another novel aspect, being the first assembly of hybrid supercapacitors using both spherical metal oxide and spherical activated carbon simultaneously.

Among various metal oxides, MnO_2 is one of the most promising pseudo-capacitive materials, due to its low cost and superior electrochemical performance.[11] In particular, the development of nanostructured MnO_2 offers the potential for further improvement in capacitance. Recently, using a

[a]*Key Laboratory for the Chemistry and Molecular Engineering of Medicinal Resources (Ministry of Education of China), School of Chemistry & Chemical Engineering of Guangxi Normal University, Guilin, 541004, P. R. China. E-mail: lzs212@163.com; 13975808173@126.com; Fax: +86 773 5854077; Tel: +86 773 3310900*
[b]*School of Metallurgical Science and Engineering, Central South University, Changsha, 410083, P. R. China*

high-surface-area carbon cathode with a positive MnO_2 anode has led to high-performance hybrid supercapacitors in aqueous electrolytes.[12] However, the cell voltages of these supercapacitors are still limited to about 2 V, which results in great importance being attached to the use of organic electrolytes to reach higher operating voltages for high specific energies. Mesocarbon microbeads (MCMBs) are a promising precursor for ACs, and have gained great attention from many researchers. They can be used to fabricate high surface area ACs (activated MCMBs or AMCMBs) by chemical activation with KOH, owing to their special lamellar crystallite structures for K intercalation.[13] These MCMB-based ACs are expected to succeed due to the spherical nature of the MCMB, which are conducive to production of high-performance supercapacitors.

Based on above analysis, in this article, we report a novel non-aqueous AMCMB|MnO_2 hybrid supercapacitor using 1 M Et_4NBF_4 in acetonitrile (AN) as an electrolyte, in order to increase the specific energy of the supercapacitor while maintaining desirable power properties. Our hybrid uses activated spherical mesocarbon microbeads, and a spherical metal oxide based on MnO_2 nanowires.

2. Experimental

Synthesis of materials

KOH chemical activation and a sonication-assisted hydrothermal synthesis were utilized to prepare the AMCMB and MnO_2, respectively. In a typical synthesis of MnO_2, 0.49 g $KClO_3$ and 0.23 g Mn_2CO_3 were dissolved in 25 mL deionized water and 15 mL concentrated HNO_3 before being sonicated for about 15 min in an ultrasonic bath, and then the mixture was transferred into a Teflon-lined stainless steel autoclave with 50 mL capacity. The autoclave was sealed and maintained at 120 °C for 12 h. After being allowed to cool to room temperature naturally, the MnO_2 product was centrifuged and washed repeatedly with distilled water to remove the excess reactants. The initial MCMBs (with an average diameter of 25 μm and a specific surface area of 32.6 $m^2\ g^{-1}$) used in the experiments were provided by Tiecheng battery Co. Ltd. (Tianjin). To enhance the specific surface area, the initial MCMBs were chemically activated by KOH: 20 g of MCMBs were mixed with 100 g of KOH in appropriate amount of distilled water, and then the mixture was heated at 2 °C min^{-1} up to 850 °C, held for 1 h in a flow of argon. After activation, the AMCMBs were centrifuged and washed with dilute HCl and distilled water in succession. Both the AMCMB and MnO_2 samples were dried under vacuum at room temperature for 24 h before characterization.

Characterization of materials

XRD patterns of the samples were recorded on a X-ray diffractometer (Rigaku, D/max 2500v/pc) with Cu-Kα_1 radiation ($\lambda = 1.5406$ Å). The 2θ range used in the measurements was from 10° to 80°. SEM images of the samples were obtained with a field-emission scanning electron microscope (Philips, FEI Quanta 200 FEG). Specific surface areas were measured by nitrogen adsorption–desorption, and pore structures were determined from the desorption branch of the nitrogen adsorption isotherm using the BJH method. The PSD was characterized by a laser diffraction particle size analyzer.

Electrochemical measurements

The MnO_2 electrodes were prepared in the form of disks (60 μm in thickness and 10 mm in diameter) by mixing 60 wt% MnO_2 in ethanol with 30 wt% of acetylene black and 10 wt% of binder (polytetrafluoroethylene, PTFE). The AMCMB electrodes were prepared by the same technique except with different weight ratios (90 wt% : 5 wt% : 5 wt%). Since MnO_2 is poorly conductive, a large amount of carbon black was used in order to decrease the ESR and thus to improve the power density. Electrochemical measurements were performed using coin-type two-electrode supercapacitor cells without a reference electrode. For the assembly of the supercapacitors, two disk-electrodes with the same mass of active materials were selected, pressed on stainless steel current collectors, and divided by a porous separator paper. A non-aqueous electrolyte, 1 M Et_4NBF_4 dissolved in acetonitrile (AN), was used in present study. The galvanostatic charge–discharge was conducted with a Battery Tester (Neware, Shenzhen, China). Cyclic voltammetry (CV) and electrochemical impedance spectroscopy (EIS) were recorded using an electrochemical workstation (ZAHNER IM6, Germany). The charge–discharge and CV were performed within voltage range of 0.0–3.0 V. The EIS were measured in the frequency range of 100 mHz to 100 kHz at an open-circuit potential with an AC perturbation of 5 mV. All measurements were performed at room temperature.

3. Results and discussion

XRD patterns of as-prepared MnO_2 and AMCMB are shown in Fig. 1. The sharp and clear diffraction peaks clearly indicate that the as-prepared MnO_2 has a good crystallinity. All the reflections of the MnO_2 can be indexed to a pure tetragonal phase [space group: *I4/m* (no. 87)] of α-MnO_2 (JCPDS 44-0141). For the AMCMB, the two weak peaks at $2\theta \approx 24°$ and 43°, corresponding to the (002) and (101) diffraction peaks (marked by ●) of carbon, are very broad and weak, which suggests that the AMCMBs have a typical amorphous structure of porous carbonaceous materials.

Fig. 2 shows the SEM images of the as-prepared samples at different magnifications. As shown by the low-magnification SEM image in Fig. 2(a), the as-prepared MnO_2 has good

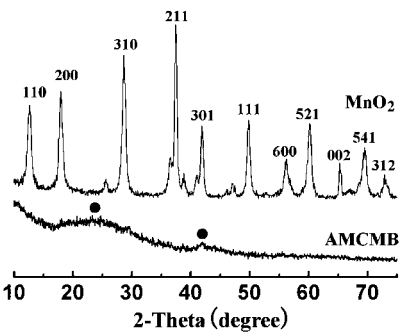

Fig. 1 XRD patterns of as-prepared MnO_2 and AMCMBs.

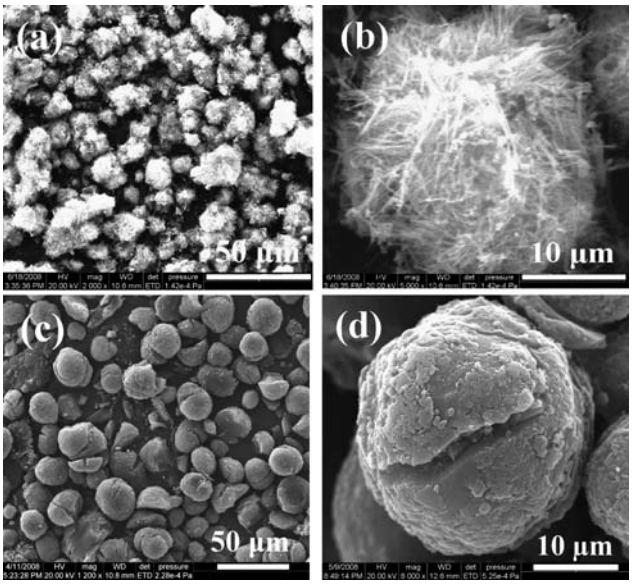

Fig. 2 SEM images of the as-prepared samples at different magnifications: (a) and (b) MnO_2 and (c) and (d) AMCMB.

a spherical morphology, with a particle diameter of 5–20 μm and a well-proportioned distribution. From the high-magnification image in Fig. 2(b), it can be seen that the MnO_2 is made up of numerous MnO_2 nanowires with diameter of 80–100 nm and length of 3–5 μm. The Brunauer–Emmet–Teller (BET) specific surface area of the MnO_2 nanowire-sphere is found to be 352 $m^2 g^{-1}$. So, it can be deduced that the nanowire-based structure of MnO_2 plays a significant role in increasing the specific surface area, which is different from those of other MnO_2 morphologies reported in the literature.[14] It is believed that the high specific surface area of one-dimensional nanostructures is conducive to the improvement of material utilization, and thus results in high faradic pseudo-capacitance in supercapacitor applications.[15]

The AMCMBs also have a good spherical distribution, with a diameter of 5–30 μm, although (as shown in Fig. 2(c)), cracks can be observed in some spheres. It is worth noting that, from the high-magnification image in Fig. 2(d), the AMCMBs have a very rough surface composed a number of nano-blocks 400–600 nm in size. Furthermore, it is observed that a "foam-like" structure is formed by the overlap and connection of the nano-blocks, which can be attributed to the etching of KOH in the high-temperature chemical activation step.[16] The AMCMBs prepared have a high mesopore volume content of 64.5% as well as a high specific surface area of 2890 $m^2 g^{-1}$. It is widely accepted that a well-developed mesopore structure of porous carbonaceous materials permits easy access for large ions to the electrode/electrolyte interface, which is crucial for supercapacitor applications in non-aqueous electrolytes.[17]

Different from the traditional hydrothermal synthesis of MnO_2, a novel two-step synthesis process was adopted in the present study: 1) the ultrasonic chemical pre-reaction and 2) the hydrothermal synthesis of MnO_2 nanowire-spheres in acidic solution. It is known that sonochemistry is an effective method for fabricating nano-materials,[18] and here this technology was used to promote MnO_2 hydrothermal synthesis by enhancing mixing of reactants in the pre-reaction process. It has been established that 1-D MnO_2 nanostructures tend to form in acidic conditions,[19] so HNO_3 was introduced as acid source in this study for the hydrothermal synthesis of MnO_2, in which Mn^{2+} could be easily oxidized into Mn^{4+} by ClO_3^- based on the following reaction:

$$Mn^{2+} + 2ClO_3^- + 4H^+ \rightarrow MnO_2 + 2H_2O + Cl_2$$

It is clear that good MnO_2 nanowire-spheres were formed effectively during the sonication–hydrothermal process from the SEM results. However, when the same hydrothermal synthesis was performed in the absence of sonication pre-reaction, rod-like MnO_2 aggregations rather than nanowire-based MnO_2 were obtained. The result suggests that the sonochemistry pre-reaction contributes to the growth of a good 1-D nanostructure and well-distributed MnO_2. It is well known that the microtexture of MCMBs can be global-type or Brooks–Taylor-type with regular lamellar structures, which favors fabrication of porous activated carbon with high surface area and controllable porous structure by chemical activation.[20] In the present study, KOH was used for activation of the MCMBs – the accepted reactions being as follows:

$$4KOH + C\ (MCMB) \rightarrow K_2CO_3 + K_2O + 2H_2 \quad (1)$$

$$K_2CO_3 + 2C\ (MCMB) \rightarrow 2K + 3CO \quad (2)$$

$$K_2O + 2C\ (MCMB) \rightarrow 2K + CO \quad (3)$$

Both this series of chemical reactions and K intercalation into the MCMB lamellar structures are critical to the achievement of a well-developed AMCMB porous structure.[21]

Particle size distribution (PSD) of electrode materials is one of the most critical parameters for the manufacturing process of energy-storage devices. It is expected that a material with more

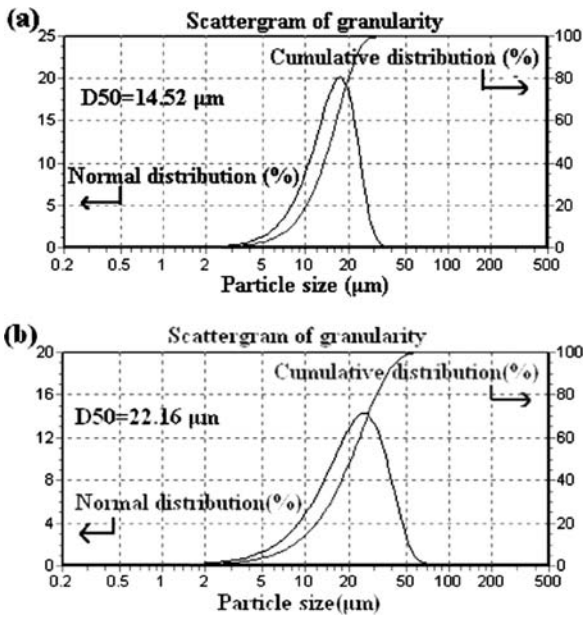

Fig. 3 Particle size distribution analysis of the as-prepared samples by laser diffraction: (a) MnO_2 and (b) AMCMB.

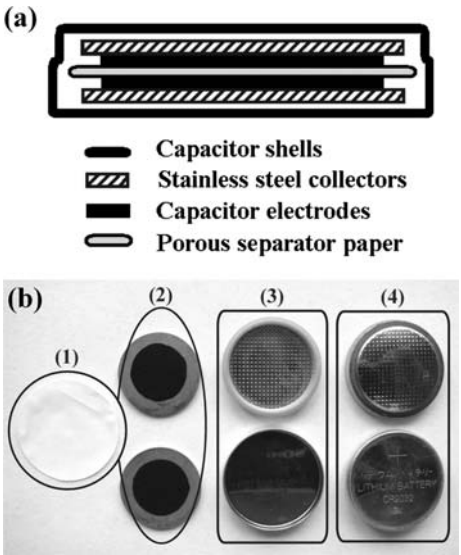

Fig. 4 (a) Schematic of the as-assembled supercapacitors. (b) Pictures of the as-assembled supercapacitors: (1) porous separator paper; (2) disk electrodes pressed on the stainless steel current collectors; (3) capacitor shells and (4) coin-type two-electrode cells.

proportioned particle size is more suitable for the production of electrodes because such a material is conducive to an increase of volumetric specific energy.[22] The PSD results of AMCMB and MnO_2 are shown in Fig. 3. It can be seen that the mean particle sizes (D_{50}) were 14.52 μm and 22.16 μm for MnO_2 and AMCMB, respectively. Both the curves are symmetric, indicating a well-proportioned PSD for the two materials, consistent with the results from the SEM images.

Electrochemical measurements were carried out using coin-type two-electrode supercapacitor cells. A schematic and pictures of as-assembled supercapacitors are shown in Fig. 4(a) and (b), respectively. The supercapacitor typically consists of two electrodes, two current collectors, one porous separator paper and two capacitor shells. The electrochemical behaviors of the supercapacitors were investigated by cyclic voltammetry, galvanostatic charge–discharge and electrochemical impedance spectroscopy. Fig. 5(a) depicts the CV curves of the AMCMB|MnO_2 hybrid supercapacitor and the AMCMB|AMCMB symmetric supercapacitor at scan rate of 10 mV s^{-1}. It is obvious that, in the potential region 0.0–3.0 V, the curve of the symmetric supercapacitor has a good rectangular shape, showing the typical capacitive property of EDLCs. For the hybrid supercapacitor, although a pair of redox peaks is observed between 1.5 and 2.0 V, the increase in CV area compared with symmetric supercapacitor indicates an improvement in capacitance.[23] The single-electrode specific capacitance (C_s) of the symmetric supercapacitor and hybrid supercapacitor calculated from CV are 176 and 228 F g^{-1}, respectively. In the symmetric supercapacitor, "the single electrode C_s" is the specific capacitance ($C_{s\text{-}AC}$) of one AMCMB electrode, which was calculated by eqn (2). In the hybrid supercapacitor, the "the single electrode C_s" is the specific capacitance average value of the AMCMB electrode and the MnO_2 electrode, the specific capacitance ($C_{s\text{-}MO}$) of one MnO_2 electrode was calculated by eqn (3).

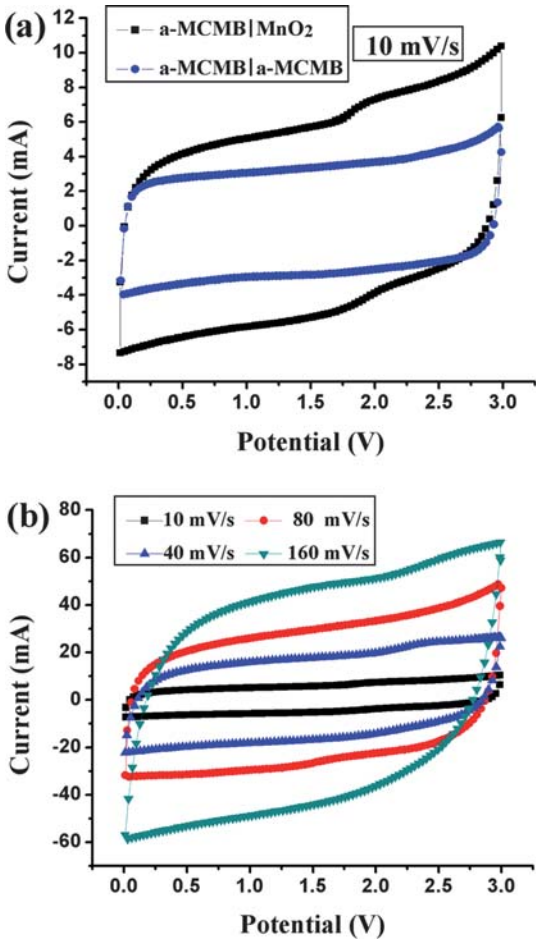

Fig. 5 Cyclic voltammograms of the as-assembled supercapacitors: (a) AMCMB|MnO_2 hybrid supercapacitor and AMCMB|AMCMB symmetric supercapacitor at a scan rate of 10 mV s^{-1} and (b) AMCMB|MnO_2 hybrid supercapacitor at different rates.

$$C_T = \frac{1}{(V_1 - V_0)} \int_{V_0}^{V_1} \frac{i(V)}{v} \, dV \quad (1)$$

$$\frac{1}{C_{T\text{-}SY}} = \frac{1}{mC_{s\text{-}AC}} + \frac{1}{mC_{s\text{-}AC}} \quad (2)$$

$$\frac{1}{C_{T\text{-}HY}} = \frac{1}{mC_{s\text{-}AC}} + \frac{1}{mC_{s\text{-}MO}} \quad (3)$$

where C_T is total series capacitance (in F) of the two-electrode supercapacitor cell (hybrid supercapacitor and symmetric supercapacitor are indicated by HY and SY respectively), i the average response current (in mA), v is the potential sweep rate (in mV s^{-1}), $(V_1 - V_0)$ represents the sweep potential range (in mV), $i(V)$ denotes the response current (in mA), m is the active mass of the single electrode, and $C_{s\text{-}AC}$ and $C_{s\text{-}MO}$ are the single electrode specific capacitance (in F g^{-1}) for the AMCMB and MnO_2, respectively. The corresponding specific energy (E_s) of symmetric supercapacitor and hybrid supercapacitor are 87 W h kg^{-1} and 128 W h kg^{-1}, respectively. The E_s values are evaluated based on

Table 1 Comparison parameters of various AC|MnO_2 hybrid supercapacitors from the literature

Cell structure	Present study	Study A[24a]	Study B[24b]	Study C[24c]	Study D[24d]
MnO_2	MnO_2 nanowire-sphere	MnO_2 powder	MnO_2 particle	MnO_2 powder	MnO_2 nanowire
AC	Spherical AMCMB	Commercial AC	Commercial AC	Commercial AC	Commercial AC
Electrolyte	1 M Et_4NBF_4 in AN	0.1 M K_2SO_4	1 M Li_2SO_4	1 M LiOH	7 M KOH
Cell voltage	3.0 V	2.0 V	2.2 V	1.5 V	1.5
Specific energy	128 W h kg^{-1}	12W h kg^{-1}	36 W h kg^{-1}	23 F g^{-1}	28 W h kg^{-1}

the total mass ($2m$) of both active materials at 3.0 V operating voltage (V) with formula $E_s = \frac{1}{2}C_T V^2/2m$. The value of specific energy almost reaches the level of rechargeable batteries, suggesting a potential application of this hybrid supercapacitor.

Currently, the majority of studies about AC|MnO_2 hybrid supercapacitors are based on aqueous electrolytes (K_2SO_4, Li_2SO_4, LiOH, KOH, *etc.*[24]). Relevant parameters of these supercapacitors are summarized in Table 1. It can be seen from Table 1 that the non-aqueous hybrid supercapacitors assembled with spherical AMCMB and MnO_2 nanowire-spheres in the present study is of great advantage in the achievement of high specific energies. The advantages are reflected in the following two aspects: high specific capacity and high operating voltage. On the one hand, the improved capacitance of the AMCMB|MnO_2 hybrid supercapacitor can reasonably be assigned to the interesting synergistic effects of these two spherical materials: 1) The high mesopore structure of AMCMB provides a preferable electrical double-layer capacitance on the basis of reversible adsorption–desorption reaction of anions on the surface of electrode material; 2) The high specific surface area of the MnO_2 nanowire-spheres could yield considerable faradic pseudo-capacitance in organic electrolytes (based on certain faradic redox reactions) which should be much higher than the electrical double-layer capacitance of ACs.[11] So, the high capacitive contribution of MnO_2 nanowire-spheres greatly improves the total capacitance of the AMCMB|MnO_2 hybrid supercapacitor. On the other hand, as shown in Table 1, the non-aqueous hybrid supercapacitors have a higher output voltage (3 V) than the aqueous counterparts ($\leq$2.2 V). The specific energy of supercapacitors is proportional to the square of cell voltage. As a result, for the AMCMB|MnO_2 hybrid supercapacitor with 1 M Et_4NBF_4 in AN, the contributions of high specific capacitance and high cell voltage lead to much higher specific energy (128 W h kg^{-1}) than those of the traditional aqueous AC|MnO_2 hybrid supercapacitors (<40 W h kg^{-1}).

In order to further examine the power performance, the CV curves of the AMCMB|MnO_2 hybrid supercapacitor at different rates (10, 40, 80 and 160 mV s^{-1}) are presented in Fig. 5(b). It can be seen that all the curves have good rectangular shapes even at a high scan rate of 160 mV s^{-1}, which indicates good rate capability and ideal power properties of the AMCMB|MnO_2 hybrid supercapacitor, allowing good kinetics in fast charge–discharge operations.[15] In addition, the corresponding C_s values of the single electrode calculated from the CV curves were about 228, 207, 185 and 162 F g^{-1} at 10, 40, 80 and 160 mV s^{-1}, respectively. These results suggest that the novel AMCMB|MnO_2 hybrid supercapacitor using 1 M Et_4NBF_4 in AN as an electrolyte is of great interest for systems requiring both high specific power and specific energy.

Table 2 The physical properties of Et_4NBF_4/AN and $LiPF_6$ (EC + DMC) electrolytes

Electrolytes	Concentration	Water content	Acid content	Main content	Conductivity
Et_4NBF_4/AN	1 M	$\leq$20 ppm	$\leq$20 ppm	$\geq$99.95%	58.2 mS cm^{-1}
$LiPF_6$/DMC + EC	1 M	$\leq$20 ppm	$\leq$40 ppm	$\geq$99.95%	12.5 mS cm^{-1}

Recently, one of our studies previously suggested that the AMCMB-based EDLCs in 1.0 M $LiPF_6$ (EC + DMC) electrolyte had an insufficient power performance.[25] For that system, the CV curve of cell was distorted severely when the scan rate only increased to 100 mV s^{-1}, which suggests that the power performance of supercapacitor is strongly determined by the nature of the electrolyte. It was reported that high ionic conductivity of electrolyte can lead to low equivalent series resistance (ESR) for supercapacitors, which affords a high specific power according to the formula: $P = V^2/(4w \times \mathrm{ESR})$, where w is the total mass of the active material.[26] The physical properties of both $LiPF_6$ and Et_4NBF_4 electrolytes in our studies are shown in Table 2. The ionic conductivity of Et_4NBF_4 in AN electrolyte is 58.2 mS cm^{-1}, which is much greater than that of $LiPF_6$ (EC + DMC) electrolyte (12.5 mS cm^{-1}). For an organic electrolyte, this is a very high conductivity value.[27] Consequently, the excellent power properties of the supercapacitor could be attributed to good ionic conductivity of electrolyte formed by dissolving Et_4NBF_4 in AN. Furthermore, the favorable one-dimensional nanostructure of MnO_2 nanowire-spheres also plays an important role in the high power performance. This is because such one-dimensional nanostructures are of great benefit to the electrolyte penetration and charge transfer due to the high surface area and high aspect ratio, resulting in facile redox reactions and fast charge–discharge for supercapacitor.[28]

Since long cycle life is of significance for supercapacitors, the electrochemical stability of AMCMB|MnO_2 hybrid supercapacitor was examined by galvanostatic charge–discharge for 1200 cycles. The cycling process was performed at a 2 mA cm^{-2} current density. The variation of C_s as a function of cycle number is shown in Fig. 6(a). The charge–discharge curve of the first six cycles is shown in the inset. The closely linear and typical trianglular distribution of the curve indicates good capacitive properties of the supercapacitor. The C_s of first cycle is 224 F g^{-1} calculated from the discharging plot according to $C = It/\Delta V$, where I is the discharge current, t is the discharge time, and ΔV is the voltage difference. The C_s value is almost consistent with that of the CV result. It is found that there is a sudden decrease in C_s value for the first 300 cycles and then the C_s remains almost constant after 300 cycles. In a word, reasonable stability of the

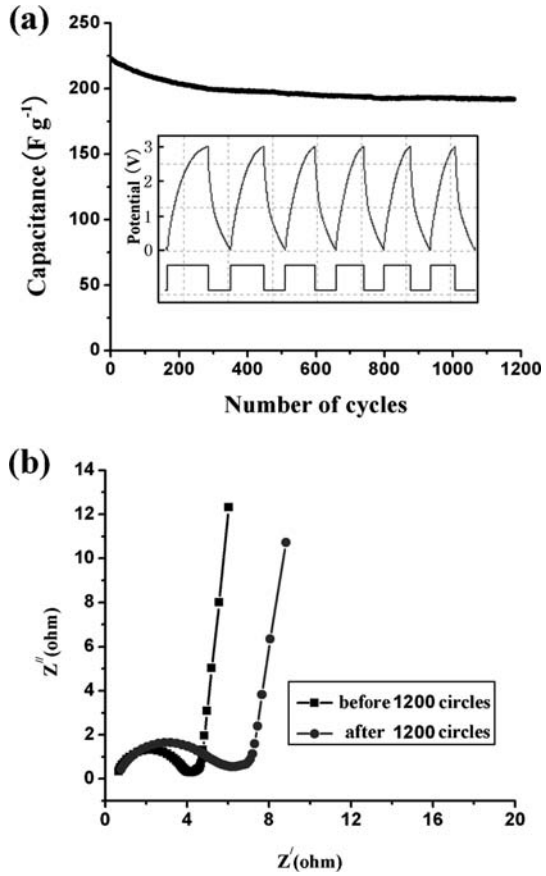

Fig. 6 The electrochemical stability of AMCMB|MnO_2 hybrid supercapacitor: (a) variation of capacitance with the number of cycles (the inset shows the galvanostatic charge–discharge curve) and (b) electrochemical impedance spectroscopy before and after 1200 cycles.

non-aqueous hybrid supercapacitor was demonstrated by the high retention (above 96%) in C_s for 1200 cycles. Fig. 6(b) shows the alternating current impedance of the AMCMB|MnO_2 hybrid supercapacitor before and after 1200 cycles. Clearly, the two impedance spectra are similar in form, namely a semicircle in the high-frequency region (reflecting the faradic pseudo-capacitance and porous structure of electrodes[29]) followed by a near-vertical line at the low-frequency region (indicating ideal capacitive behavior of the supercapacitors[30]). A difference between the two spectra is that, after 1200 cycles, the charge transfer resistance (R_{ct}) has increased from 3.95 Ω to 4.68 Ω, which is probably attributable to the loss of some active materials from the current collector or the dissolution of some MnO_2 in the repeating charge–discharge operations. More detailed characterization and testing methods are in progress, in order to optimize the performances of the AMCMB|MnO_2 hybrid supercapacitor.

4. Conclusions

Two kinds of spherical materials, spherical AMCMB and MnO_2 nanowire-spheres, were synthesized and used in AMCMB|MnO_2 hybrid supercapacitor for energy-storage applications. The as-prepared AMCMB and MnO_2 have good spherical morphologies and relatively well-proportioned size distributions. The electrochemical performance of the AMCMB|MnO_2 hybrid supercapacitor was characterized by cyclic voltammograms, AC impedance and charge–discharge testing in 1 M Et_4NBF_4/AN. According to the voltage value of 3.0 V, the C_s of the hybrid supercapacitor was 228 F g^{-1} at 10 mV s^{-1} scan rate, with the hybrid supercapacitor having a much higher specific energy than that of the symmetric one. Moreover, good rate capability, ideal power properties as well as desirable cycling stability are demonstrated for the AMCMB|MnO_2 hybrid supercapacitor. All these results persuade us to propose this novel hybrid supercapacitor as a promising candidate for energy-storage applications.

Acknowledgements

Financial support by the National Natural Science Foundation of China (Nos. 20663001 and 20763002) and the R&D Project (GUIJINENG 05112001-2D and GUIKEGONG 0992001-1) are gratefully acknowledged.

References

1 (*a*) D. Qu, *J. Power Sources*, 2002, **109**, 403; (*b*) M. Winter and R. J. Brodd, *Chem. Rev.*, 2004, **104**, 4245; (*c*) D. Choi, G. E. Blomgren and P. N. Kumta, *Adv. Mater.*, 2006, **18**, 1178.
2 R. Kotz and M. Carlen, *Electrochim. Acta*, 2000, **45**, 2483.
3 J. M. Tarascon and M. Armand, *Nature*, 2001, **414**, 359.
4 (*a*) V. Ganesh, S. Pitchumani and V. Lakshminarayanan, *J. Power Sources*, 2006, **158**, 1523; (*b*) T. Brousse, R. Marchand, P. L. Taberna and P. Simon, *J. Power Sources*, 2006, **158**, 571; (*c*) Q. Wang, Z. Wen and J. Li, *Adv. Funct. Mater.*, 2006, **16**, 2141.
5 T. Brousse, R. Marchand, P. L. Taberna and P. Simon, *J. Power Sources*, 2006, **158**, 571.
6 (*a*) A. Lewandowski and M. Galinski, *J. Power Sources*, 2007, **173**, 822; (*b*) M. Galinski, A. Lewandowski and I. Stepniak, *Electrochim. Acta*, 2006, **51**, 5567; (*c*) P. L. Taberna, P. Simon and J. F. Fauvarque, *J. Electrochem. Soc.*, 2003, **150**, A292.
7 (*a*) A. Laforgue, P. Simon, J. F. Fauvarque, M. Mastragostino, F. Soavi, J. F. Sarrau, P. Lailler, M. Conte, E. Rossi and S. Saguatti, *J. Electrochem. Soc.*, 2003, **150**, A645; (*b*) P. W. Ruch, R. K. and A. Wokaun, *Electrochim. Acta*, 2009, **54**, 4451; (*c*) J. Zhao, C. Lai, Y. Dai and J. Xie, *Mater. Lett.*, 2007, **61**, 4639; (*d*) M. Mastragostino and F. Soavi, *J. Power Sources*, 2007, **174**, 89.
8 K. T. Nam, D. W. Kim, P. J. Yoo, C. Y. Chiang, N. Meethong, P. T. Hammond, Y. M. Chiang and A. M. Belcher, *Science*, 2006, **312**, 885.
9 (*a*) S. I. Lee, S. Mitani, S. H. Yoon, Y. Korai and I. Mochida, *Carbon*, 2004, **42**, 2332; (*b*) J. F. Ni, H. H. Zhou, J. T. Chen and X. X. Zhang, *Mater. Lett.*, 2007, **61**, 1260.
10 (*a*) H. Chen, J. M. Wang, T. Pan, Y. L. Zhao, J. Q. Zhang and C. N. Cao, *J. Power Sources*, 2005, **143**, 243; (*b*) X. Cao, J. Wei, Y. Luo, Z. Zhou and Y. Zhang, *Int. J. Hydrogen Energy*, 2000, **25**, 643; (*c*) M. Yoshio, H. Wang and K. Fukuda, *Angew. Chem., Int. Ed.*, 2003, **42**, 4203; (*d*) K. T. Lee, Y. S. Jung and S. M. Oh, *J. Am. Chem. Soc.*, 2003, **125**, 5652.
11 P. Simon and Y. Gogotsi, *Nat. Mater.*, 2008, **7**, 845.
12 T. Brousse, P. L. Taberna, O. Crosnier, R. Dugas, P. Guillemet and Y. Scudeller, *J. Power Sources*, 2007, **173**, 633.
13 (*a*) Z. M. Shen and R. S. Xue, *Fuel Process. Technol.*, 2003, **84**, 95; (*b*) R. S. Xue and Z. M. Shen, *Carbon*, 2003, **41**, 1862.
14 (*a*) C. Yuan, B. Gao, L. Su and X. Zhang, *J. Colloid Interface Sci.*, 2008, **322**, 545; (*b*) R. N. Reddy and R. G. Reddy, *J. Power Sources*, 2004, **132**, 315.
15 J. H. Kim, T. Ayalasomayajula, V. Gona and D. Choi, *J. Power Sources*, 2008, **183**, 366.
16 Z. M. Shen and R. S. Xue, *Fuel Process. Technol.*, 2003, **84**, 95.
17 (*a*) C. T. Hsieh and Y. T. Lin, *Microporous Mesoporous Mater.*, 2006, **93**, 232; (*b*) E. R. Thomas, H. J. Denisa, E. Fiset, Z. H. Zhu and G. Q. Lu, *Electrochem. Commun.*, 2009, **11**, 974.

18 (*a*) N. A. Dhas, Y. Koltypin and A. Gedanken, *Chem. Mater.*, 1997, **9**, 3159; (*b*) M. Hibino, H. Zhou and I. Honma, *J. Power Sources*, 2005, **146**, 304.
19 N. Kijima, H. Yasuda, T. Sato and Y. Yoshimura, *J. Solid State Chem.*, 2001, **159**, 94.
20 (*a*) J. D. Brooks and G. H. Taylor, *Carbon*, 1965, **3**, 185; (*b*) Y. B. Ji, T. H. Li, L. Zhu, X. X. Wang and Q. Lin, *Appl. Surf. Sci.*, 2007, **254**, 506.
21 C. Lu, S. Xu, Y. Gan, S. Liu and C. Liu, *Carbon*, 2005, **43**, 2295–2301.
22 (*a*) X. Z. Fu, Q. C. Xu, R. Z. Hu, B. X. Pan, J. D. Lin and D. W. Liao, *J. Power Sources*, 2007, **164**, 916; (*b*) J. Ying, M. Lei, C. Jiang, C. Wan, X. He, J. Li, L. Wang and J. Ren, *J. Power Sources*, 2006, **158**, 543.
23 R. K. Sharma, H. S. Oh, Y. G. Shul and H. S. Kim, *J. Power Sources*, 2007, **173**, 1024.
24 (*a*) T. Brousse, P. L. Taberna, O. Crosnier, R. Dugas, P. Guillemet and Y. Scudeller, *J. Power Sources*, 2007, **173**, 633; (*b*) Y. Xue, Y. Chen, M. L. Zhang and Y. D. Yan, *Mater. Lett.*, 2008, **62**, 3884; (*d*) A. Yuan and Q. Zhang, *Electrochem. Commun.*, 2006, **8**, 1173; (*d*) X. Y. Wang, X. Wang, T. Hou, J. Li and Q. Huang, *J. Chem. Ind. Eng. (China)*, 2006, **57**, 442.
25 H. Wang, Z. Li, J. Yang, Qingyu Li and X. Zhong, *J. Power Sources*, 2009, **194**, 1218.
26 (*a*) M. Mastragostino and F. Soavi, *J. Power Sources*, 2007, **174**, 89; (*b*) K. C. Ng, S. Zhang, C. Peng and G. Z. Chen, *J. Electrochem. Soc.*, 2009, **156**, A846.
27 K. S. Ryu, K. M. Kim, Y. J. Park, N. G. Park, M. G. Kang and S. H. Chang, *Solid State Ionics*, 2002, **152–153**, 861.
28 (*a*) M. H. Huang, S. Mao, H. Feick, H. Q. Yan, Y. Y. Wu, H. Kind, E. Weber, R. Russo and P. D. Yang, *Science*, 2001, **292**, 1897; (*b*) S. Chou, J. Wang, S. Chew, H. Liu and S. Dou, *Electrochem. Commun.*, 2008, **10**, 1724.
29 J. Gamby, P. L. Taberna, P. Simon, J. F. Fauvarque and M. Chesneau, *J. Power Sources*, 2001, **101**, 109.
30 M. Toupin, D. Bélanger, I. R. Hill and D. Quinn, *J. Power Sources*, 2005, **140**, 203.